VTT Technical Research Centre of Finland

Effect of the fluid flow fragmentation on the hydrothermal performance enhancement of a serpentine mini-channel heat sink

Jaffal, Hayder Mohammad; Freegah, Basim; Hussain, Ammar A.; Hasan, Ala

Published in:
Case Studies in Thermal Engineering

DOI:
10.1016/j.csite.2021.100866

Published: 01/04/2021

Document Version
Publisher's final version

Case Studies in Thermal Engineering 24 (2021) 100866

Contents lists available at ScienceDirect

Case Studies in Thermal Engineering

journal homepage: http://www.elsevier.com/locate/csite

Effect of the fluid flow fragmentation on the hydrothermal performance enhancement of a serpentine mini-channel heat sink

Hayder Mohammad Jaffal [a], Basim Freegah [a], Ammar A. Hussain [a], Ala Hasan [b,*]

[a] Mechanical Engineering Department, College of Engineering, Mustansiriyah University, Baghdad, Iraq
[b] VTT Technical Research Centre of Finland Ltd., P.O.Box 1000, FI-02044, VTT, 1, Finland

HIGHLIGHTS

- Novel design of SMCHS is proposed based on flow fragmentation.
- Flow fragmentation plays a vital role in the reduction of pressure drop through SMCHS.
- Hydrothermal performance of SMCHS is significantly improved using flow fragmentation.
- SMCHS with orthogonal segmentation showed better overall performance than that with diagonal segmentation.
- The overall performance of the SMCHS with segmentation increases with increasing the cooling water mass flow rate.

ARTICLE INFO

Keywords:
Serpentine mini-channel
Nusselt number
Flow fragmentation
pressure drop
hydrothermal performance

ABSTRACT

This paper aims to investigate the effect of fluid flow fragmentation on the hydrothermal performance characteristics of a serpentine mini-channel heat sink (SMCHS) numerically and experimentally. Two novel designs, namely, perpendicular and diagonal, which are related to where the fluid flow is fragmented in the SMCHS, are investigated. The two new designs have two entrances and two exits. The flow in each entrance is divided into two branches. In the current study, 3D CFD ANSYSIS–Fluent program is used in the numerical simulations. The three designs, namely, one conventional and the two novel designs, were manufactured and tested to validate the reliability of the numerical simulations and to compare the performance experimentally. The analysis of the results shows that the flow fragmentation effectively improves the SMCHS characteristics compared with the conventional SMCHS. Moreover, the outcomes indicate that the improved heat transfer of the fragmentation disperser, represented by the Nusselt number, increases by 13% accompanied by a reduction in the pressure drop by about 180% compared with the conventional design. The new SMCHS with the perpendicular fragmentation design is found to be slightly better than that with the diagonal fragmentation design.

1. Introduction

Among the various heat sinks, mini-channel heat sink (MCHS) is an effective way to remove unwanted high heat fluxes generated from electronic devices, especially when using water as a cooling medium. One of the most important types of MCHSs is serpentine mini-channel heat sink (SMCHS), which has been used in several important applications, such as electronic equipment and fuel cells.

* Corresponding author.
E-mail addresses: jaffal.env@uomustansiriyah.edu.iq, hayder.jaffal@gmail.com (H.M. Jaffal), basim.freegah@uomustansiriyah.edu.iq (B. Freegah), ammar.smf1974@uomustansiriyah.edu.iq (A.A. Hussain), ala.hasan@vtt.fi (A. Hasan).

https://doi.org/10.1016/j.csite.2021.100866
Received 17 September 2020; Accepted 23 January 2021
Available online 31 January 2021

Recently, as a result of the rapid development of electronic devices, the issue of improving the performance of micro/mini-channel heat sinks has become a challenge for researchers. Li et al. [1] numerically simulated the channel geometry using multi-optimization algorithm to optimize a serpentine channel heat sink (SCHS) under turbulent flow conditions. They studied the impacts of the width of the channel, aspect ratio and turn clearance on the minimization of the thermal resistance and pressure drop of the heat sink. Hao et al. [2] proposed a simple model for the thermal resistance to simulate the thermal characteristics of SMCHS at Reynolds number less than 500. They studied the impacts of channel aspect ratio and fluid Reynolds number on the hydrothermal performance of SMCHS. Hao et al. [3,4] conducted a numerical study validated by experimental testing of the performance of the SMCHS to predict the characteristics of the pressure gradient and thermal resistance. The study was conducted to show the effect of the loss coefficient of the bend, ratio of the channel height to width, fin thickness and the clearances of the turn under the Reynolds number range of 500–1500. Al-Neama et al. [5] numerically and experimentally investigated the performance characteristics of the SMCHS to evaluate their suitability for Gallium Nitride thermal management at transformers with high mobility power. To reduce hot spots, the heat spreader is placed above the heating source. The impacts of the water flow rate, spreader material and spreader thickness on the reduction the maximum heat flux and temperature of chip were investigated. Al-Neama et al. [6] studied the performance of a new type of SMCHS by using chevron fins to create secondary flow at a certain angle in the original path to reduce the heat resistance and pressure drop. The effects of different parameters, such as channel number, channel width, oblique angle, flow rate and heat flux, on the hydrothermal characteristics of a SMCHS are evaluated numerically and experimentally. Imran et al. [7] studied the effect of the flow distribution on the improvement of the performance of a conventional SMCHS using two serpentine channels with two inputs and outputs and different flow configurations rather than a single serpentine channel. The effects of the flow configuration, heat flux and mass flow rate on the thermal and hydraulic characteristics of the SMCHS were studied numerically and experimentally. Fernando et al. [8] proposed various unconventional patterns of liquid-cooled SCHS. Their new flow patterns consist of an inlet flow in the center of the heat sink to feed the radial serpentine channels and several flow outlets on the outside of the heat sink. Different cases were studied numerically by changing the channel number, channel length and spiral number. Based on the temperature uniformity on the heating surface, the heat sink thermal performance is compared with all flow patterns. Chen et al. [9] performed a multi-objective structural design of SCHS. In the structural modeling of the SCHS, the following design variables were defined: channel number, channel height, channel width, fin width, inlet water velocity and input and output locations to reduce the thermal resistance and pressure drop of the SCHS. The experimental and numerical results achieved the structure model of the channels and the water velocity at the inlet, thereby ensuring a smaller thermal resistance and lower pressure drop. Vajravel et al. [10] conducted numerical and experimental studies on the thermal performance of a new MCHS involving four parts, each equipped with inlet and outlet for cooling water and rectangular channels with two bends in each channel. The flow in the MCHS is divided in four entrances and exits, which contribute to the high reduction in the temperature difference compared with the conventional rectangular MCHS under the same laminar flow conditions. Zhang et al. [11] numerically and experimentally investigated the transient thermal characteristics of liquid cooling for electronic chip using rectangular micro-channel heat sink. The heat sink is analyzed with three different channel configurations, namely, straight, serpentine, and U-shape. For the different channels, the impacts of flow rate and heat flux on the

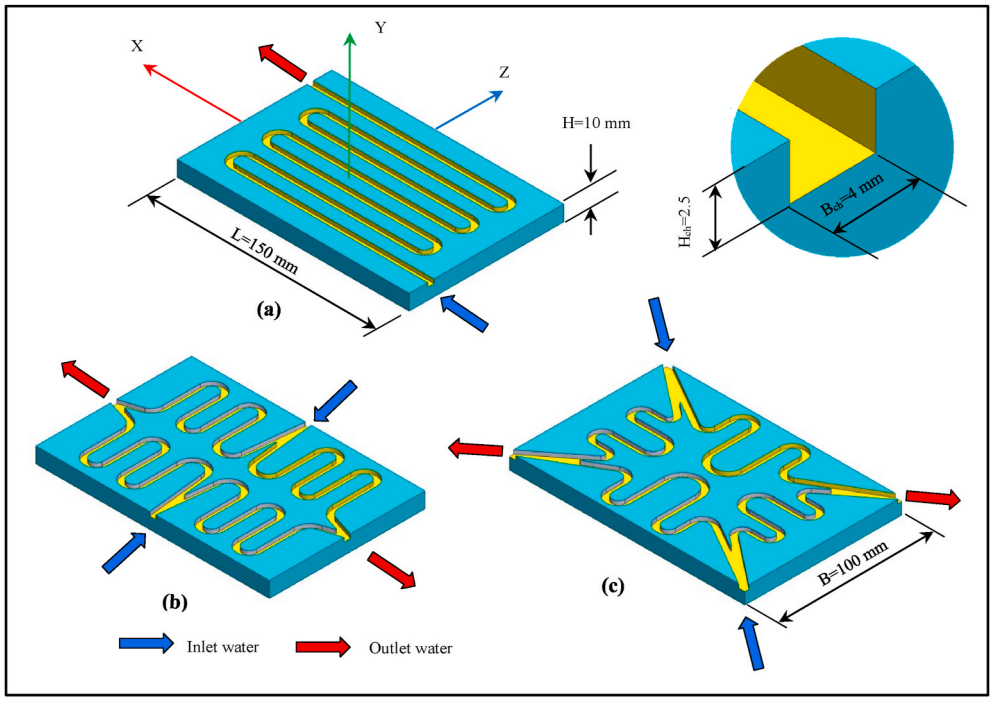

Fig. 1. Schematic of the SMCHSs (a) Conventional, (b) Design A (orthogonal arrangement) and (c) Design B (diagonal arrangement).

temperature changes over the time were studied. The influence of using secondary channels for connecting the main channel through turning along the length on the performance of the laminar water flow inside SMCHS is studied numerically by Singh et al. [12]. Different secondary channel angles were examined, and the effect on the pressure drop and Nusselt number of SMCHS is investigated. They reported that the secondary flow with angle of 40° provides minimum pressure drop compared with the conventional SMCHS, whereas the angle of 10° gives maximum Nusselt number. Sivakumar et al. [13–15] conducted an experimental and theoretical study on the fluid flow and heat transfer characteristics of serpentine micro-channel heat sink using nanofluids. The effects of the hydraulic diameter, Reynolds number, heat input, type of nanofluids and nanofluid concentration on performance were studied.

Despite the large volume of literature devoted to analyzing the thermal performance of heat-sink mini-channel, the effect of the flow fragmentation on the characteristics of the fluid flow and heat transfer of the SMCHS has not been explicitly analyzed. Most of the research work is devoted to studying the effect of the various parameters, such as the configuration of the channel, mass flow rate and heat flux. Almost all of these studies focused on the improvement of the thermal performance, but the increase in the pressure drop was not considered. Hence, most of these improvements are accompanied with high pressure drop. Accordingly, the present work endeavors to fill the research gaps in the aforementioned area by suggesting two new designs of SMCHS and by studying the effect of the flow fragmentation on the hydrothermal performance through an experimental study backed by CFD modeling. The two new designs have two inlets and two outlets to assure uniform temperature distribution on the surface of the heat sink. All the cases are conducted under various boundary conditions regarding the heat flux and mass flow rate of the working fluid under laminar flow conditions. In addition, experimental tests are conducted to validate the reliability of the numerical simulation, as well as to compare the overall hydrothermal performance (Nusselt number and pressure drop) for the models under study.

2. Problem description

The conventional SMCHS, as shown in Fig. 1a, consists of one channel with one inlet and one outlet; a corrugated path passes through alternating turns along the heat sink. It is characterized by its high thermal performance as an inevitable result of the continuous mixing of runoff at the turns. At the same time, it is characterized by the negative effect on the hydraulic performance as a result of the increase of the pressure drop through the heat sink, which requires a high pumping power. The results of Imran et al. [7] indicated that the dividing the flow into two serpentine channels instead of one serpentine channel plays an important role in improving the performance of SMCHS. Therefore, to improve the overall performance, flow fragmentation in the SMCHS should be based on the two following principles: (1) better flow distribution tends to improve the heat transfer, as it ensures a better heat exchange with the entering cooling water; and (2) it reduces the pumping power of the cooling liquid. The pumping power is proportional to the pressure drop, and the pressure drop increases with increasing the channel path length. New channel configurations can be developed using these two principles. Therefore, two new models are proposed in the current work, namely, orthogonal flow and diagonal flow arrangements regarding the inlet and outlet flow to the SMCHS. The difference between the conventional model (serpentine) and proposed models is in the number of inlets and outlets of the working fluid, as shown in Fig. 1b and c. Despite this difference, the same length of the track is maintained in the proposed models compared with the conventional model.

3. Numerical method

3.1. Physical model of the SMCHS

The geometrical parameters of all SMCHSs under consideration in this study can be defined as follows: length of SMCHS (L = 150 mm), width of SMCHS (B = 100 mm), height of SMCHS (H = 10 mm), channel width (B_{ch} = 4 mm) and channel height (H_{ch} = 2.5 mm). The heat dissipated from the electronic chip is represented by a constant heat flux applied on the bottom surface of the SMCHS. The heat transfer is from the lower surface to the solid (copper) by conduction and then rejected from the surface of the channels to the cooling fluid (water) by forced convection. For conventional SMCHS, the Reynolds number for cooling liquid is less than 1100. 3D heat transfer and fluid flow for SMCHS are solved under the assumptions of single-phase incompressible, Newtonian fluid, steady-state, laminar flow. Furthermore, the radiation dissipation effects, body forces and gravity are not considered.

3.2. Conservation equations and boundary conditions

The governing equations for continuity, momentum, and energy are listed as follows [16,17]:

3.2.1. - Continuity equation

$$\nabla.\vec{U} = 0 \tag{1}$$

3.2.2. - Momentum equation

$$\nabla.\vec{U}\vec{U} = -\frac{1}{\rho_w}\nabla P + v_w\nabla^2.\vec{U} \tag{2}$$

3.2.3. - Energy equations

$$\nabla.\vec{U}T = \frac{k_w}{\rho_w C_{P,w}}\nabla^2.T \quad (water) \tag{3}$$

$$k_c\nabla^2.T = 0 \quad (copper) \tag{4}$$

where $\vec{U}$ is the velocity vector. P, ρ, υ, C_P, T and k are the pressure, density, kinematic viscosity, specific heat, temperature and thermal conductivity, respectively.

To solve the abovementioned governing equations, several assumptions are defined for the fluid and solid domains of the heat sink. Water is assumed to be the cooling fluid with a constant inlet temperature of 293 K and constant velocity. Based on the desired mass flow rates, the inlet water velocity is calculated. At the outlet, the pressure is assumed to be atmospheric pressure. Copper is used as the material of the heat sink. For all heat sink walls, a no-slip boundary condition is applied. Also, the outer walls of the heat sink are assumed to be perfectly insulated with the exception of the bottom wall, which is exposed to uniform heat flux. The heat flux between the solid and the liquid is equal at the walls of the channels. Table 1 shows details of the applied hydrothermal boundary conditions and their locations.

3.3. Simulation implementation

ANSYS fluent 18 program is utilised for the simulation of the fluid flow and heat transfer through the SMCHS. The computational domains for water and copper are partitioned into a large number of unstructured grids. For all the SMCHSs designs under study, tetrahedral grids are used to provide high accuracy with minimal calculation time. Fig. 2 represents the grid-generated sampled for the SMCHS design B simulation. The governing equations with the defined boundary conditions are solved by the finite volume method. To solve the differential equations for the combined pressure and velocity, the SIMPLE algorithm is used. By using the order upwind, the convective and diffuse terms are discretised. For all the considered variables, when the residual values are less than 10^{-6}, the simulation calculations are approved.

3.4. Grid sensitivity

The accuracy of the numerical solution is highly dependent on the quality of the grid. Thus, to ensure the results' sensitivity to the nature of the grid, an independent study of the grid is conducted. At the flow rate of 0.001 kg/s and heat flux of 12 kW/m^2, the sensitivity of five different numbers of grids ranging from 0.45 to 1 million is tested based on the results of the Nusselt number. Table 2 summarises the tests conducted for the three studied SMCHSs designs. The Nusselt number difference decreases by increasing the number of grids. The grid number is adopted when the difference in the Nusselt number reaches less than 1x10^{-4}, which was found to be 0.843, 0.712 and 0.958 million for the conventional serpentine, design A and design B, respectively.

4. Experimental method

4.1. Experimental test rig

The test rig under study consists of the following main parts: test clip, heat sink, heat exchanger, water tank, water pump, globe

Table 1
Hydrothermal boundary conditions.

	Thermal boundary condition			Hydraulic boundary condition		
	Conventional	Design A	Design B	Conventional	Design A	Design B
Inlet (x,y,z) in mm	$T = T_{in} = 293\ K$			$\overline{u} = \overline{u}_{in}$ $\overline{v} = \overline{w} = 0$		
	(-75,7.5, -36)	(0,7.5,+50) (0,7.5,-50)	(+75,7.5,+50) (-75,7.5,-50)	(-75, 7.5,-36)	(0,7.5,+50) (0,7.5,-50)	(+75,7.5,+50) (-75,7.5,-50)
Outlet (x,y,z) in mm	$\frac{\partial^2 T_f}{\partial x^2} = 0$			$P_{out} = 1\ atm$		
	(+75,7.5,+36)	(+75,7.5,0) (-75,7.5,0)	(+75,7.5,-50) (-75,7.5,+50)	(+75,7.5,+36)	(+75,7.5,0) (-75,7.5,0)	(+75,7.5,-50) (-75,7.5,+50)
Interface surfaces	$k_f\frac{\partial T_f}{\partial n} = k_S\frac{\partial T_S}{\partial n}$			$\overline{u} = \overline{v} = \overline{w} = 0$		
Top surface	$k_f\frac{\partial T_f}{\partial n} = 0,\ k_f\frac{\partial T_f}{\partial n} = 0$			$\overline{u} = \overline{v} = \overline{w} = 0$		
Lower surface	$q'' = constant$			$\overline{u} = \overline{v} = \overline{w} = 0$		
Other surface	$k_f\frac{\partial T_f}{\partial n} = 0\ ,\ k_f\frac{\partial T_f}{\partial n} = 0$			$\overline{u} = \overline{v} = \overline{w} = 0$		

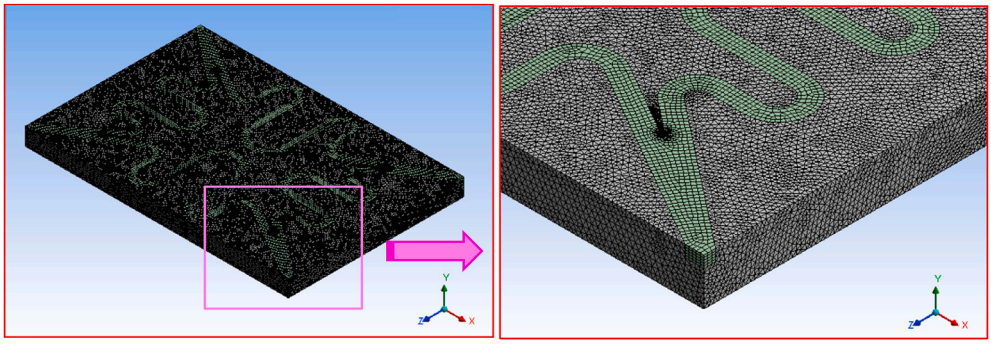

Fig. 2. Grid distribution for design B: (a) whole computational domain, (b) near the flow inlet.

Table 2
Grid sensitivity test on the Nusselt number at mass flow rate 0.001 kg/s and heat flux 12 kW/m.^{2}.

No		1	2	3	4	5
Conventional	Grid number	475393	569305	658259	724008	843639
	Nusselt number	9.0961	8.995	8.895	8.7821	8.782
	Nusselt number difference	0.314	0.213	0.113	0.00009	0
Design A	Grid number	360813	461805	584659	660113	712193
	Nusselt number	9.751	9.603	9.1972	9.1971	9.197
	Nusselt number difference	0.554	0.406	0.0002	0.0001	0
Design B	Grid number	403684	492646	598483	711494	958419
	Nusselt number	9.4677	9.395	9.273	9.18609	9.186
	Nusselt number difference	0.2997	0.191	0.015	0.00009	0

valve, flow meter, digital manometer to measure pressure, thermocouples for temperature measurement, data logger, dispersion heating system, tubes and connectors, as shown in Fig. 3. The purpose of the water pump is to circulate the cooling water within the whole experimental rig, i.e. from storage tank to test section, then to the heat exchanger and return back to the tank. The type of this mini-pump is GP-3360, and it works by 220 V and 50 Hz. The maximum flow rate is 500 L/h (0.138 kg/s of water). To control and measure the flow rate of the cooling water, the globe valve and the flow meter are used, respectively. The flow meter under study can measure flow rates between 3 and 30 L/h with an error of ±0.2%. Digital manometer (PDMM01) was used to measure the pressure drop between the inlet and outlet of the heat sink with accuracy of ±0.3%. The material of SMCHSs under study is copper, with general

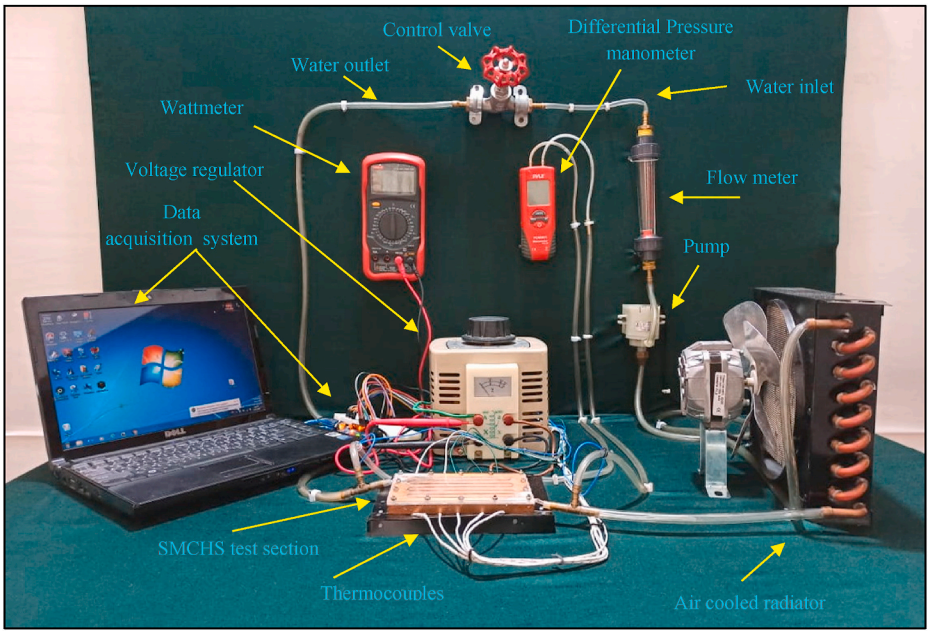

Fig. 3. The experimental set-up.

dimensions of 150 mm long, 100 mm wide and 10 mm deep. The height and width of the channel are 2.5 and 4 mm, respectively. Fig. 4 is a photo of the heat sinks under study: the conventional model and the two new designs A and B, which are manufactured using CNC machine. Therefore, Fig. 4 shows the final form of the test section assembly. To minimize heat loss from the test section, an insulation layer was added on the bottom surface of the heat sink. The test section is equipped with 12 thermocouples type K with an error of ±0.3 °C, 10 thermocouples to measure the temperature of the SMCHS base and two thermocouples to measure the water temperature at the inlet and outlet. All thermocouples were calibrated before installation into the specified locations. Furthermore, a data logger is used to measure the temperatures and to record them on a personal laptop. To provide a clear view of the flow field within the dispersion channels, a transparent Perspex cap is installed on the top surface of the dispersion. An electric heater is installed on the lower surface of the heat sink to supply power to the test section and ensure a uniform heat flux to the heat sink. The amount of heat supplied is controlled using a voltage regulator. The voltage and current were measured using the multi-action meter. The water is pumped at ambient temperature to enter the disperser and then acquires heat as it passes through the dispersion channels. To cool the water that exits from the dispersion before returning to the tank, a heat exchanger with finned tubes is used. In addition, all the measuring instruments used to test dispersion performance were calibrated before installing them. Data required at a flow rate from 0.001 kg/s to 0.0025 kg/s were tested to ensure that the flow is still laminar. Firstly, to start the test, the tank is filled with water. Then, the pump is turned on, and the flow rate is adjusted by using the globe valve. Secondly, the heater is turned on, and the voltage and current are adjusted. The water inlet temperature is fixed at 293 K during the test by using the heat exchanger. A sufficient duration of time is set between the readings to ensure a steady state of the test depending on the flow rate and heat flux under the study. Afterwards, the voltage, current, inlet and outlet temperatures of water, dispersion base temperature, pressure drop and flow rate are recorded. These steps are repeated for each studied flow rate and heat flux. All previous steps are repeated for all dispersions under study.

4.2. Uncertainties analysis of the experimental measurements

To ensure the reliability and accuracy of the results obtained from the experimental work, error analysis is carried out. Every measurement device used has a certain inaccuracy. The calculation of the total uncertainty is analyzed using the following equation [18,19]:

$$U_R = \left[\sum_{i=1}^{i=N} \left(\frac{\partial R}{\partial x_i} u_i \right)^2 \right]^{1/2} \tag{5}$$

where, u_i is the uncertainty of the independent variables.

Accordingly, the uncertainties of heat gain, Nusselt number, heat transfer coefficient, thermal resistance and pumping power can be defined as follows:

Heat gain ($\dot{Q}_w$):

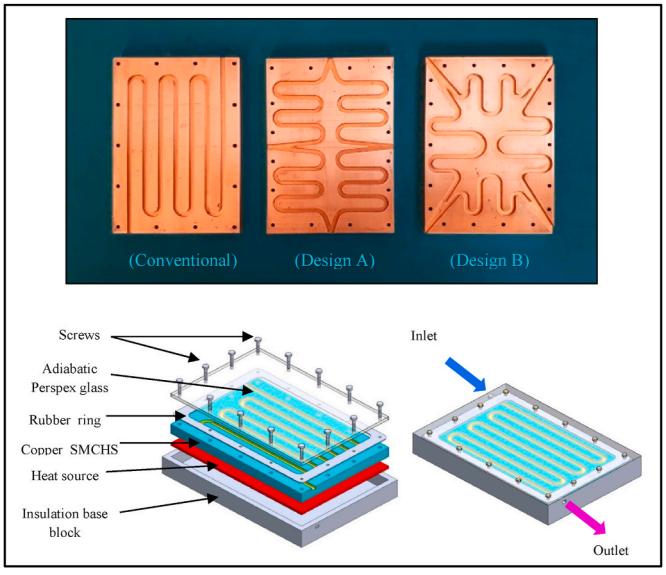

Fig. 4. Fabricated test SMCHSs and schematic diagram of the conventional SMCHS test section assembly.

$$\frac{U\dot{Q}_w}{\dot{Q}_w}=\left[\left(\frac{u\rho_w}{\rho_w}\right)^2+\left(\frac{u\dot{V}}{\dot{V}}\right)^2+\left(\frac{uC_{pw}}{C_{pw}}\right)^2+\left(\frac{u\left(T_{w,o}-T_{w,i}\right)}{\left(T_{w,o}-T_{w,i}\right)}\right)^2\right]^{½} \tag{6}$$

Logarithmic mean temperature difference (LMTD):

$$\frac{ULMTD}{LMTD}=\left[\left(\frac{u\left(T_{w,o}-T_{w,i}\right)}{\left(T_{w,o}-T_{w,i}\right)}\right)^2+\left(\frac{u\left(T_{b,av}-T_{w,i}\right)}{\left(T_{b,av}-T_{w,i}\right)}\right)^2+\left(\frac{u\left(T_{b,av}-T_{w,o}\right)}{\left(T_{b,av}-T_{w,o}\right)}\right)^2\right]^{½} \tag{7}$$

Heat transfer coefficient ($\overline{h}$):

$$\frac{U\overline{h}}{\overline{h}}=\left[\left(\frac{u\dot{Q}_w}{\dot{Q}_w}\right)^2+\left(\frac{uA_{ch}}{A_{ch}}\right)^2+\left(\frac{uLMTD}{LMTD}\right)^2\right]^{½} \tag{8}$$

Nusselt number ($\overline{Nu}$):

$$\frac{U\overline{Nu}}{\overline{Nu}=\left[\left(\frac{u\overline{h}}{\overline{h}}\right)^2+\left(\frac{uk_w}{k_w}\right)^2\right]^{½}} \tag{9}$$

Thermal resistance (θ):

$$\frac{U\theta}{\theta}=\left[\left(\frac{uLMTD}{LMTD}\right)^2+\left(\frac{u\dot{Q}_w}{\dot{Q}_w}\right)^2\right]^{½} \tag{10}$$

Pumping power (Wp):

$$\frac{UWp}{Wp}=\left[\left(\frac{u\dot{V}}{\dot{V}}\right)^2+\left(\frac{u\Delta P}{\Delta P}\right)^2\right]^{½} \tag{11}$$

Using the abovementioned equations and by relying on Table 3, which includes the inaccuracy of the various physical variables measured directly, the total error ratios are calculated for all the studied performance determinants and as follows: Nusselt number Nu 4.87%, the coefficient of heat transfer h 4.77%, the thermal resistance θ 4.76%, and the pumping power Wp 11.2%. From the presented uncertainty analysis, it can be concluded that the error in the measurements of the performance parameters is within an acceptable range.

5. Results and discussion

5.1. Comparisons between the numerical and experimental results

To verify the accuracy and credibility of the numerical simulation model, three comparisons are conducted for the results obtained experimentally under the same geometry and operating conditions (heat flux of 12 kW/m^2) for the conventional design, design A and design B, as shown in Fig. 5. The pumping power required to circulate cooling water during SMCHS can be expressed in terms of pressure drop and volumetric flow rate [20], as follows:

$$W_p=\dot{V}\times\Delta P \tag{12}$$

Table 3
Uncertainty of the experimental measurement parameters.

Parameter	Uncertainty (%)
ρ_w	±1
k_w	±1
$C_{p,w}$	±1
A	±0.2
$(T_{b,av}-T_{w,i})$	±1.7 to ±6
$(T_{b,av}-T_{w,o})$	±1.7 to ±6
$(T_{w,o}-T_{w,i})$	±0.6 to ±3
ΔP	±2 to ±11
$\dot{V}$	±0.3 to 2.5

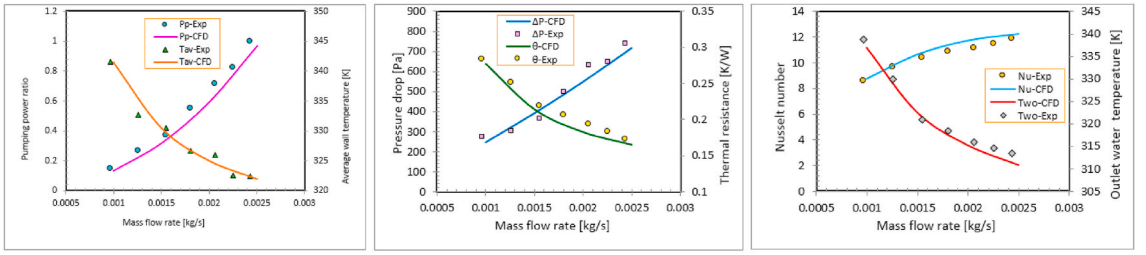

(a) Conventional

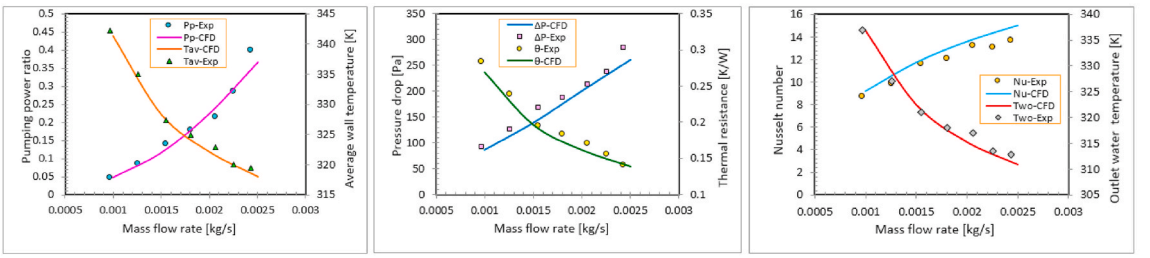

(b) Design A

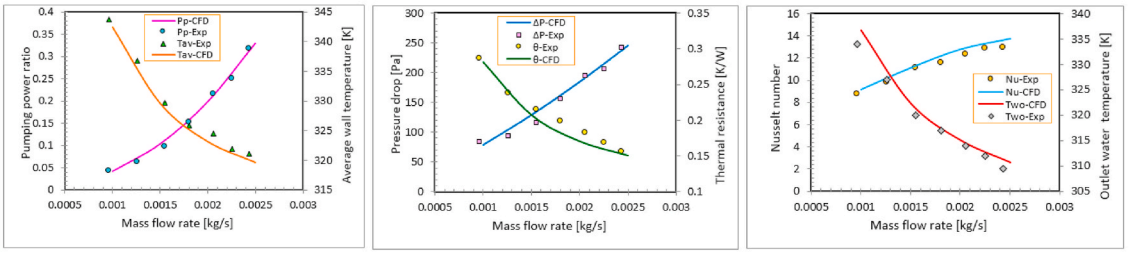

(c) Design B

Fig. 5. Comparisons between the results of the numerical simulation and experimental test for different channel designs.

where $\dot{V}$ is the volumetric flow rate of water. ΔP is the pressure drop through the channels of the heat sink. Fig. 5 (left) shows good convergence between the numerical and experimental results in the general behavior as well as the values of the pumping power ratio (Pumping power/maximum pumping power of the conventional SMCHS) and average wall temperature distribution under various mass flow rates of the cooling water. Furthermore, Fig. 5 reports that the maximum deviation between the experimental and numerical results of the pumping power ratio is 10.5%, 10.4% and 5.6% for the conventional design, design A and design B, respectively. The deviation of the average surface temperature is 1.54%, 1.98% and 1.89% for the conventional design, design A and design B, respectively. According to the above, the highest difference between the experimental and numerical results is recorded with the pumping power ratio, whereas the lowest difference is recorded with the temperatures. The reason for this is the fact that the pumping power depends on two variables, which are the pressure drop and the flow rate, whereas the temperature depends on one variable. Thus, the error increases as a result of the accumulation of composite errors.

The overall thermal resistance is an important indicator typically used to evaluate the thermal performance of the MCHS and can be defined as follows [21,22]:

$$\theta = \frac{LMTD}{\dot{Q}_w} \tag{13}$$

where LMTD is logarithmic mean temperature difference and Q_w is the heat gain. Fig. 5 (middle) depicts the comparison between the numerical and experimental results for the pressure drop and the thermal resistance. This figure shows a good convergence between the numerical and experimental results. Moreover, the maximum difference percentages for pressure drop are 8.9%, 10.83% and 5.62% for the conventional design, design A and design B, respectively. The percentage differences of the thermal resistance are 3.4%, 3% and 4% for the conventional design, design A and design B, respectively.

One of the most important parameters used in evaluating the thermal performance of heat sinks is the Nusselt number, which is a

non-dimensional number representing the ratio between the convection heat transfer to the conduction heat transfer. Eq. (14) can be used to estimate the average Nusselt number [23]:

$$\overline{Nu} = \frac{\overline{h} D_h}{k_w} = \frac{\dot{Q}_w D_h}{A_{ch}(LMTD)k_w} = \frac{\dot{m}_w C_{p,w}\left(T_{w,o} - T_{w,i}\right) D_h}{A_{ch}(LMTD)k_w} \tag{14}$$

where $\overline{h}$is the average convection heat transfer coefficient, Q_w is the heat gain, D_h is the hydraulic diameter of the channel, A_{ch} is the heat transfer area, k_w is the water thermal conductivity, m_w is the water mass flow rate, C_{pw} is the water specific heat, $T_{w,o}$ is the outlet water temperature and $T_{w,i}$ is the inlet water temperature. Fig. 5 (right) shows the comparison between the numerical and experimental results of the Nusselt number and the exit temperature of the cooling water. This figure shows that the convergence between the numerical and experimental results is significantly good: the maximum error percentages for the number of Nusselt are 2.5%, 4.7% and 3.7% and for the exit water temperature are 3.52%, 3.08% and 3.92% for the conventional design, design A and design B, respectively. According to the above findings, we can state that reasonable differences exist between the numerical and experimental results for all models and parameters under study. Plausible explanations for the differences could be the thermal losses, measurement errors and numerical assumptions. For all the studied parameters, the maximum difference between the numerical results and the experimental measurements is found to be less than 11%. Therefore, the developed numerical approach is considered accurate enough and can be applied to the investigation of heat transfer simulations and fluid flow of the heat sink, thereby leading to the prediction of the hydrothermal performance of the heat sink mini-channel.

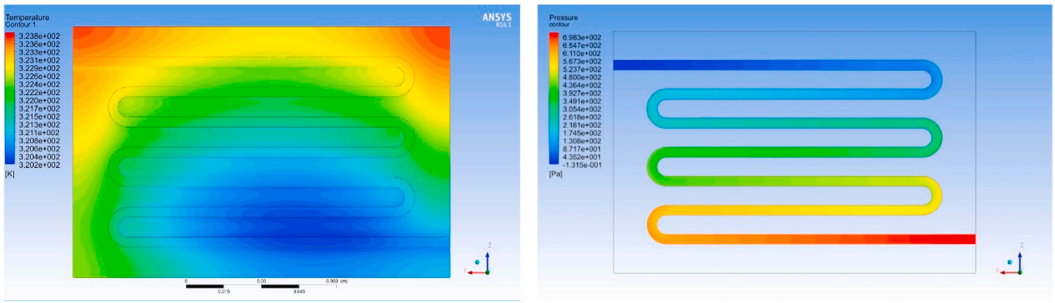

(a) Conventional

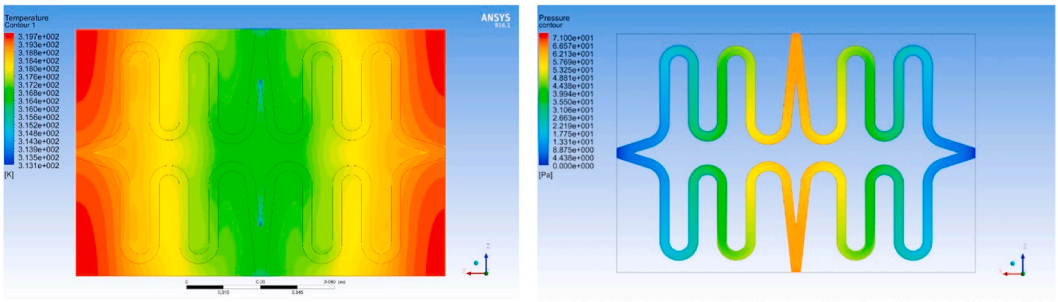

(b) Design A

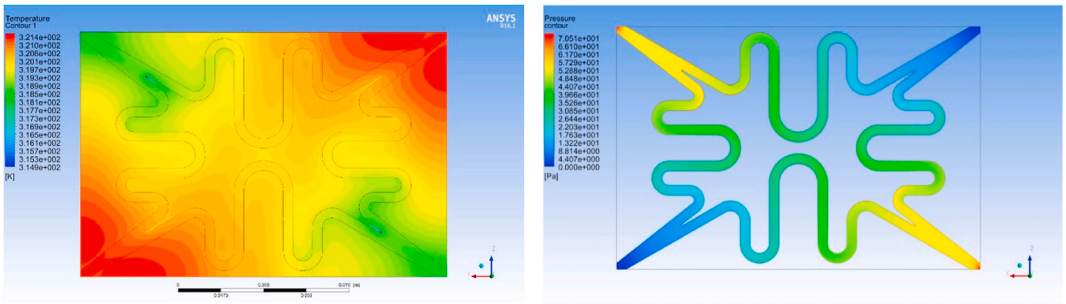

(c) Design B

Fig. 6. Temperature distribution in the solid domain (left) and Pressure distribution of the fluid domain (right) for the three SMCHSs under a heat flux of 12 kW/m^2 and a mass flow rate of 0.0025 kg/s.

5.2. Numerical results

Fig. 6 depicts the numerical results for the temperature and pressure drop counters of the heat sink for all models considered in this study at a mass flow rate of 0.0025 kg/s and a heat flux of 12 kW/m^2. The minimum heat sink temperature is at the channel inlet, and the temperature increases gradually up to the outlet of channel. The increase in the temperature of the cooling water during the passage in the channel of heat sink leads to a reduction in the heat transfer rate. Furthermore, this figure shows that flow fragmentation has an effect on the reduction of the heat sink temperature. Flow fragmentation in the new models leads to more contact between the cooled water and the hot region of the heat sink, thereby resulting in better temperature uniformity of the heat sink and increased rate of heat transfer. Hence, the thermal stresses are reduced. In addition, increase of channel curves in the new models enhanced the mixing of the cooling water, thereby contributing effectively to the reduction of the maximum temperature of the heat sink. Although the temperature in the region of the outlet in the new models is higher as compared with other regions of the heat sink, the temperature of this region is lower than that of the conventional model. For instance, in comparison with conventional SMCHS, the maximum temperature reductions for designs A and B are 4.1 and 2.4 K, respectively. A higher pressure drop happens at the inlet region of the heat sink for all models, and it decreases gradually, reaching its least value at the outlet region. In addition, the pressure drop value for the new models is about three times smaller than that of the conventional model. This result is due to the fact that the flow fragmentation improves the hydraulic performance of the heat sink significantly. The advantage of the two proposed models is the presence of two inlets, which leads to the division of the flow and the reduction of the velocity of the cooling water in each channel, thereby reducing the hydraulic friction loss. This in turn reduces the total pressure drop of the heat sink. Furthermore, very small differences exist between the proposed designs (A and B) regarding pressure drop.

Fig. 7 shows the variation of the Nusselt number with the a mass flow rate of the cooling water under heat flux values of 6 kW/m^2 and 12 kW/m^2. The Nusselt number increases with increasing the mass flow rate of the cooling water for all models considered in the present study. The reason behind this is the increase in the heat transfer rate by convection within the channel of the heat sink. Furthermore, the Nusselt number for the three models at the lower mass flow rate is smaller compared with the higher mass flow rate. In addition, the Nusselt number of both new models is larger compared with that of the conventional model. This thermal enhancement becomes more apparent at the higher flow rate for which the ratio of the Nusselt number enhancement (Nusselt number of modified SMCHS/Nusselt number of conventional SMCHS) reaches 1.23 and 1.12 for the proposed designs A and B, respectively. The Nuesselt number enhancement ratio is almost equal for the two heat fluxes. Comparatively, under constant flow rate, a noticeable increase in the Nusselt number is observed with the higher heat flux, however, this increase is not remarkable compared with the increase in the Nusselt number caused by the increased flow rate.

According to these results, flow fragmentation orthogonally or diagonally has a small effect on the pressure drop, as observed from Fig. 8. This figure shows the effect of the flow rate on the pressure drop for all cases under consideration and shows that the increase of the flow rate leads to an increase in the pressure drop for all cases. The flow fragmentation means that rather than using a long single channel path, the flow is divided into four short paths by splitting the flow into two parts. Then, every part is divided into two branches. This process effectively reduces the friction force of the flow, which in turn reduces the pressure drop. In addition, this decrease of pressure drop due to the new design becomes more effective when flow rates are increased. The pressure drop ratio (pressure drop through the modified SMCHS/pressure drop through the conventional SMCHS) decreases by approximately 2.7 and 3 for the proposed designs A and B, respectively; however, the difference in the pressure drop between the two new models is small.

The effective improvement of the cooling thermal performance of the proposed SMCHS as compared to the conventional SMCHS

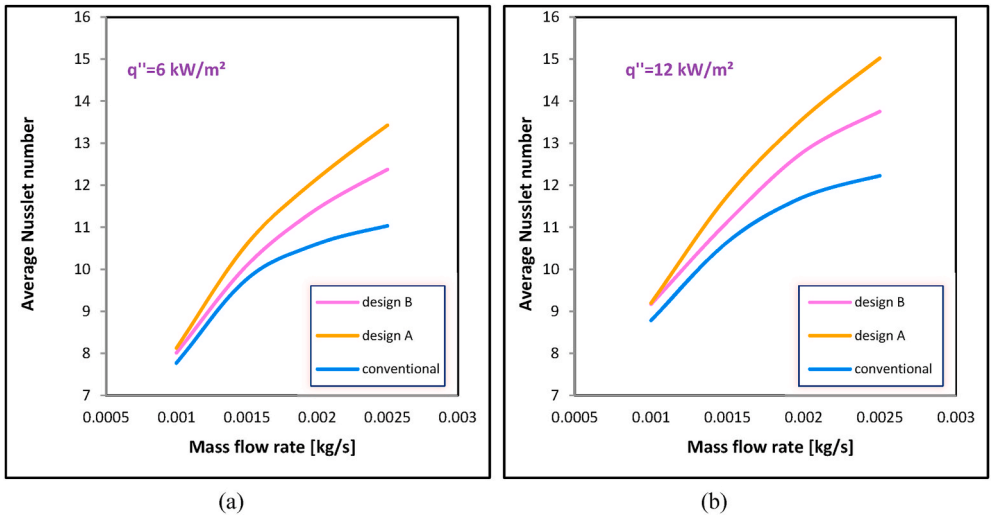

Fig. 7. Influence of the channel design on the average Nusselt number for different mass flow rates; (a) under a heat flux of 6 kW/m^2 and (b) under a heat flux of 12 kW/m^2.

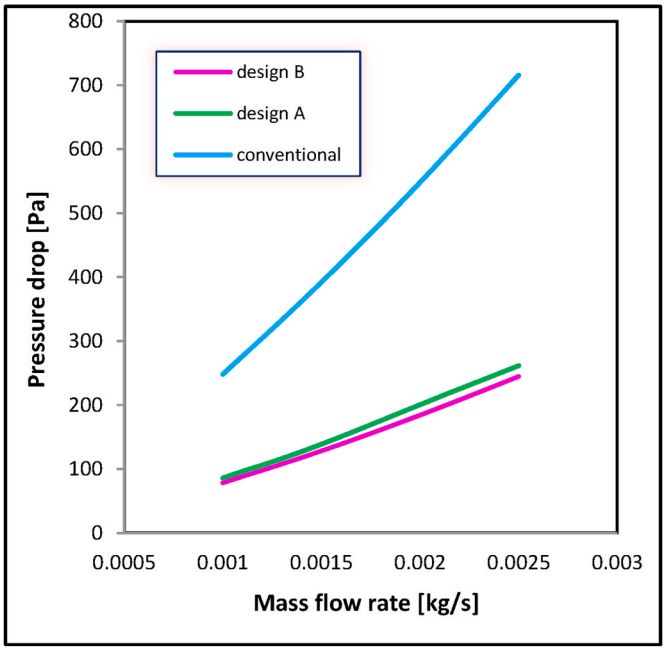

Fig. 8. Influence of the channel design on the pressure drop for different mass flow rates.

based on the enhancement of the average Nusselt number ratio relative to the pressure drop ratio is given by the overall hydrothermal performance factor (OHPF). The OHPF is calculated by Eq. (15) [24,25].

$$\mathrm{OHPF} = \overline{\mathrm{Nu}}_{\mathrm{ESMCHS}} \Big/ \overline{\mathrm{Nu}}_{\mathrm{CSMCHS}} \Big/ \sqrt[3]{\Delta\ \mathrm{P}_{\mathrm{ESMCHS}} / \Delta\ \mathrm{P}_{\mathrm{CSMCHS}}} \tag{15}$$

where $\mathrm{Nu}_{\mathrm{ESMCHS}}$ is the Nusselt number of the modified SMCHS, $\mathrm{Nu}_{\mathrm{CSMCHS}}$ is the Nusselt number of the conventional SMCHS, $\Delta \mathrm{P}_{\mathrm{ESMCHS}}$ is the pressure drop through the modified SMCHS, and $\Delta \mathrm{P}_{\mathrm{CSMCHS}}$ is the pressure drop through the conventional SMCHS. According to Figs. 7 and 8, which represent the Nusselt number and pressure drop, respectively, the best performance of the heat sink regarding enhancement the heat transfer with minimum pressure drop can be determined. Table 4 shows the variation in the overall hydrothermal performance factor OHPF, which is calculated from Eq. (15) at various mass flow rates of the cooling water for the new models. For the two proposed SMCHSs, the table emphasises that the flow fragmentation effectively contributes to the improvement of the overall performance of the heat sink. For heat flux 12 kW/m^2 and at the highest flow rate, the OHPF is about 1.72 and 1.62 for designs A and B, respectively, compared with the conventional SMCHS. The overall performance factor increases with increasing the mass flow rate despite the increase in the pressure drop. The pressure drop in both new models is lower than that in the conventional model, as shown in Fig. 8. Thus, the denominator of the equation becomes smaller, which leads to an increase in the performance factor. Furthermore, the Nusselt number enhancement increases with the increasing flow rate, whereas the ratio of the pressure drop decreases. Hence, the performance factor increases accordingly. At the lowest flow rate, it is noted that design B has a higher OHPF than design A, but when the flow continues to increase, design A has higher OHPF. The reason for this is due to the fact that the rate of improvement in heat transfer is close at the lowest flow rate, but the pressure drop of design B is relatively smaller than that of design A. However, with the increase in the flow rate, it is clearly noted that the heat transfer improvement of design A is higher compared to

Table 4
Comparison of the overall hydrothermal performance factor (OHPF) between designs A and B; (a) under a heat flux of 6 kW/m^2 and (b) under a heat flux of 12 kW/m.^{2}.

Mass flow rate [kg/s]	Overall hydrothermal performance factor (OHPF)			
	Design A		Design B	
	6 kW/m^2	12 kW/m^2	6 kW/m^2	12 kW/m^2
0.001	1.489	1.490	1.514	1.532
0.0015	1.534	1.559	1.498	1.516
0.002	1.602	1.621	1.551	1.570
0.0025	1.702	1.719	1.604	1.609

design B. For different passive heat transfer improvement techniques of the MCHSs, the OHPF decreases with increasing the mass flow rate of the cooling water, as mentioned in previous studies [26,27]. However, the results of the current study show the opposite in terms of the pressure drop. Design A has the best OHPF under all mass flow rates in this study. A large convergence of the OHPF values exists under the two values of heat flux as shown in Table 4. The reason for this is the convergence of the values of the ratio of Nusselt number enhancement.

5.3. Experimental results

To further demonstrate the effect of the flow fragmentation on the overall thermal performance, the thermal resistance of and pumping power ratio the new SMCHSs is compared with that of the conventional SMCHS. Fig. 9a demonstrates the effect of the mass flow rate on the thermal resistance for all SMCHSs under study. This figure confirms that flow fragmentation effectively contributes to the reduction of thermal resistance, which results in improved thermal performance. At a higher flow rate, the decrease in the thermal resistance are approximately 23% and 10.5% for designs A and B, respectively, compared with the conventional SMCHS. The thermal resistance declines as the flow rate increases due to the increase in the rejected heat, which is in inverse relationship with the thermal resistance (reduced average surface temperature). Furthermore, design A has a lower thermal resistance compared with design B for all mass flow rates under consideration. The main aim of the performance improvement of any micro/min-channel heat sink is to achieve the highest heat dissipation with the lowest pressure drop, thereby ensuring the lowest pumping power [28]. Variations of the pumping power ratio (Pumping power/maximum pumping power of the conventional SMCHS) for the studied SMCHSs under various mass flow rates are illustrated in Fig. 9b. As expected, the pumping power increases with increasing the flow rate for all cases in the study due to the increase in both the pressure drop and flow rate. A remarkable decrease in pumping power is seen for designs A and B compared with the conventional SMCHS at the same flow rate. The reason for the decrease in pumping power is the decrease in flow resistance within the new SMCHS caused by the flow fragmentation. The most important advantage that makes the new design of the SMCHS better than the conventional design is the apparent decrease in pumping power. The pumping power difference increases dramatically with increasing the flow rate. The decrease of the pumping power for designs A and B is estimated to be 294% and 353% respectively, compared with the conventional model. However, the effect of flow rate on the pumping power of the conventional SMCHS is higher compared with those of the new models. An exponential increase in the pumping power is observed with increasing the flow rate of the conventional SMCHS, whereas the increase in new SMCHSs is almost linear. Thus, at high flow rates, the flow fragmentation is an ideal solution to reduce the high pumping power. The difference in the pumping power for designs A and B is very small, however, design B shows a slight lower pumping power than design A.

6. Conclusions

The aim of this investigation is to study the effect of the fluid flow fragmentation on the hydrothermal performance characteristics of a serpentine mini-channel heat sink (SMCHS) under laminar flow conditions. Two novel designs were investigated, a perpendicular (orthogonal) design and a diagonal design, related to how the fluid flow is fragmented in the SMCHS, named as design A and design B, respectively. The flow fragmentation in the two new designs is made by making two entrances and two exits of the cooling water, where the flow in each entrance is then divided into two branches. The performance of the new designs were compared, numerically and experimentally, with a conventional design that has one entrance and one exit.

Based on the results of numerical and experimental analyses, the following conclusions can be made:

1. In general, the thermal resistance and pumping power are greatly reduced due to the fragmentation of the flow compared with single flow under the same operational conditions.
2. The flow fragmentation contributes to a more uniform temperature distribution on the surface of the SMCHS.
3. In comparison with the conventional SMCHS, the heat transfer is enhanced effectively when the flow of the heat sink is fragmented. Such enhancement becomes more apparent at high flow rates. Accordingly, under heat flux of 12 kW/m^2, the ratio of Nusselt number enhancement (Nusselt number of modified SMCHS/Nusselt number of conventional SMCHS) reaches 1.23 and 1.12 for the proposed designs A and B, respectively.
4. The pressure drop of the cooling water is effectively reduced when the flow is fragmented in the SMCHS. The pressure drop ratio (pressure drop through modified SMCHS/pressure drop through conventional SMCHS) decreases by approximately 2.7 and 3 for the proposed designs A and B, respectively.
5. Under the same mass flow rate, the overall hydrothermal performances of the new SMCHS models (with fragmented flow) are much better compared with the conventional SMCHS. This improvement in the overall hydrothermal performance is proportional to the flow rate. Compared with the conventional SMCHS under heat flux of 12 kW/m^2 and at the highest flow rate, the OHPF increased 1.72 times for design A and 1.62 for design B, respectively.

Declaration of competing interest

The authors declare that they have no known competing financial interests or personal relationships that could have appeared to influence the work reported in this paper.

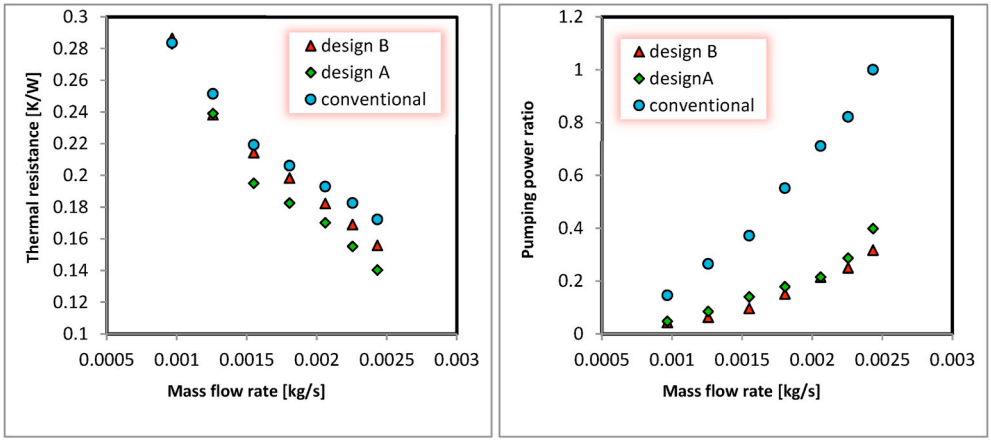

Fig. 9. Influence of the channel design on (a) thermal resistance and (b) pumping power ratio for different mass flow rates.

Acknowledgment

The authors would like to thank Mustansiriyah University (https://www.uomustansiriyah.edu.iq), Baghdad-Iraq, for the given support in accomplishing the present work.

References

[1] X. Li, X. Hao, Y. Chen, M. Zhang, B. Peng, Multi-objective Optimizations of Structural Parameter Determination for Serpentine Channel Heat Sink, 2013, pp. 449–458. European Conference on the Applications of Evolutionary Computation, Applications of Evolutionary Computation.
[2] X.H. Hao, X.K. Li, B. Pen, M. Zhang, Y. Zhu, Thermal resistance network model for heat sinks with serpentine channels, Int. J. Numer. Model. Electron. Network. Dev. Field. 27 (2014) 298–307.
[3] X.H. Hao, B. Peng, G. Xie, Y. Chen, Thermal analysis and experimental validation of laminar heat transfer and pressure drop in serpentine channel heat sinks for electronic cooling'', ASME, J. Electron. Packag. 136 (2014) 1–9.
[4] X.H. Hao, Z. Wu, X. Chen, Experimental Study of Heat Transfer and Pressure Drop in Serpentine Channel Water Cooler Heat Sink', 16th International Conference on Fluid Mechanics, Heat Transfer and Thermodynamics, Canada, Toronto, 2014. June 16-17.
[5] A.F. Al-Neama, N. Kapur, J. Summers, H.M. Thompson, Thermal management of GaN HEMT devices using serpentine minichannel heat sinks, Appl. Therm. Eng. 140 (2018) 622–636.
[6] A.F. Al-Neama, Z. Khatir, N. Kapur, J. Summers, H.M. Thompson, An experimental and numerical investigation of chevron angle in serpentine minichannel heat sinks, Int. J. Heat Mass Tran. 120 (2018) 1213–1228.
[7] A.A. Imran, N.S. Mahmoud, H.M. Jaffal, Numerical and experimental investigation of heat transfer in liquid cooling serpentine mini-channel heat sink with different new configuration models, Therm. Sci. Eng. Progr. 6 (2018) 128–139.
[8] F. Cano-Banda, U.C. Gonzalez-Valle, S. Tarazona-Cardenas, A. Hernandez-Guerrero, Effect of different geometry flow pattern on heat sink performance '', papers presented to the 12th international conference on heat transfer, fluid mechanics and thermodynamics, Costa de Sol, Spain on (2016) 419–424, 11-13 July.
[9] Y. Chen, B. Peng, X. Hao, G. Xie, Fast approach of Pareto-optimal solution recommendation to multi-objective optimal design of serpentine-channel heat sink, Appl. Therm. Eng. 70 (2014) 263–273.
[10] L.V. Vajravel, S.K. Swaminathan, S. Baskaran, R.K. Sekar, Experimental investigations on heat transfer in a new minichannel heat sink, Int. J. Therm. Sci. 140 (2019) 144–153.
[11] J. Zhang, T. Zhang, S. Prakash, Y. Jaluria, Experimental and numerical study of transient electronic chip cooling by liquid flow in microchannel heat sinks, Numer Heat TR A-APPL. 65 (2014) 627–643.
[12] V. Singh, H.C. Das, P. Nemalipuri, Numerical analysis of heat transfer and fluid flow in mini-channel heat sink with interconnecting channels, Adv. Mech. Eng. (2020) 987–1000.
[13] A. Sivakumar, N. Alagumurthi, T. Senthilvelan, Heat transfer enhancement of serpentine shaped micro channel heat sink with Al_2O_3 water nanofluid, Int. J. Tech. Res. Appl. 2 (2015) 112–116.
[14] A. Sivakumar, N. Alagumurthi, T. Senthilvelan, Investigation of heat transfer in serpentine shaped microchannel using Al_2O_3/water nanofluid, Heat Tran. Asian Res. 45 (2014) 1–10.
[15] A. Sivakumar, N. Alagumurthi, T. Senthilvelan, Effect of CuO/water nanofluid heat transfer in serpentine shaped microchannel heat sink, Int. J. Mech. Therm. 5 (2014) 1–10.
[16] D. Yang, Y. Wang, G. Ding, Z. Jin, J. Zhao, G. Wang, Numerical and experimental analysis of cooling performance of single-phase array microchannel heat sinks with different pin-fin configurations, Appl. Therm. Eng. 112 (2017) 1547–1556.
[17] X.Y. Li, S.L. Wang, X.D. Wang, T.H. Wang, Selected porous-ribs design for performance improvement in double-layered microchannel heat sinks, Int. J. Therm. Sci. 137 (2019) 616–626.
[18] C.J. Ho, W.C. Chen, An experimental study on thermal performance of Al_2O_3/water nanofluid in a minichannel heat sink, Appl. Therm. Eng. 50 (2013) 516–522.
[19] F.S. Moghanlou, A.S. Khorrami, E. Esmaeilzadeh, H. Aminfar, Experimental study on electrohydrodynamically induced heat transfer enhancement in a minichannel, Exp. Therm. Fluid Sci. 59 (2014) 24–31.
[20] S.E. Ghasemi, A.A. Ranjbar, M.J. Hosseini, Thermal and hydrodynamic characteristics of water-based suspensions of Al_2O_3 nanoparticles in a novel minichannel heat sink, J. Mol. Liq. 230 (2017) 550–556.
[21] M. Saeed, M.H. Kim, Heat transfer enhancement using nanofluids (Al_2O_3-H_2O) in mini-channel heat sinks, Int. J. Heat Mass Tran. 120 (2018) 671–682.
[22] A.A. Awais, M.H. Kim, Experimental and numerical study on the performance of a minichannel heat sink with different header geometries using nanofluids'', Appl. Therm. Eng. 171 (2020) 115125.
[23] M.R. Sohel, S.S. Khaleduzzaman, R. Saidur, A. Hepbasli, M.F.M. Sabri, I.M. Mahbubul, An experimental investigation of heat transfer enhancement of a minichannel heat sink using Al_2O_3–H_2O nanofluid, Int. J. Heat Mass Tran. 74 (2014) 164–172.

[24] H. Liu, D. Qi, X. Shao, W. Wang, An experimental and numerical investigation of heat transfer enhancement in annular microchannel heat sinks, Int. J. Therm. Sci. 142 (2019) 106–120.
[25] T.C. Hung, X. HuangY, W.M. Yan, Thermal performance analysis of porous-microchannel heat sinks with different configuration designs, Int. J. Heat Mass Tran. 66 (2013) 235–243.
[26] M. Attalla, M. Hussein Maghrabie, E. Specht, An experimental investigation on fluid flow and heat transfer of rough mini-channel with rectangular cross section, Exp. Therm. Fluid Sci. 75 (2016) 199–210.
[27] C. Bi, G.H. Tang, W.Q. Tao, Heat transfer enhancement in mini-channel heat sinks with dimples and cylindrical grooves, Appl. Therm. Eng. 55 (2013) 121–132.
[28] D.R.S. Raghuraman, R.T.K. Raj, P.K. Nagarajan, B.V.A. Rao, Influence of aspect ratio on the thermal performance of rectangular shaped micro channel heat sink using CFD code, Alexandria Eng. J. 56 (2017) 43–54.

Nomenclatures

Ac_h: heat transfer area, mm^2
B: SMCHS width, mm
B_{ch}: channel width, mm
Cp: specific heat, $Jkg^{-1}K^{-1}$
D_h: hydraulic diameter$2(B_{ch} \times H_{ch})/(B_{ch} + H_{ch})$, mm
H: SMCHS height, mm
H_{ch}: channel height, mm
$\overline{h}$: coefficient of heat transfer, $\frac{\dot{Q}_w}{A_{ch}LMTD}$,$Wm^{-2}\ K^{-1}$
k: thermal conductivity, $Wm^{-1}K^{-1}$
L: SMCHS length, mm
$LMTD$: log mean temperature difference $\frac{(T_{b,av}-T_{w,i})-(T_{b,av}-T_{w,o})}{ln[(T_{b,av}-T_{w,i})/(T_{b,av}-T_{w,o})]}$, K
$\dot{m}_w$: water mass flow rate, $\rho_w \dot{V}$, kgs^{-1}
$\overline{Nu}$: Nusselt number, $\frac{\overline{h}D_h}{k_w}$, -
$OHPC$: overall hydrothermal performance coefficient
P: pressure, Pa
ΔP: pressure drop $(P_i - P_o)$, Pa
$\dot{Q}_w$: heat gain $\rho_w \dot{V} C_{pw}(T_{w,o} - T_{w,i})$, W
Re: Reynolds number, $\frac{\rho_w \overline{u} D_h}{\mu_w}$
$T_{w,m}$: mean water temperature$0.5(T_{w,o} - T_{w,i})$, K
T_b: heat sink bottom wall temperature, K
$\overline{u}$: average velocity, $m\ s^{-1}$
$\dot{V}$: volume flow rate, $L\ min^{-1}$
Wp: pumping power$\dot{V} \times nP$, kWGreek Symbols
ρ: density, $kg\ m^{-3}$
ν: kinematic viscosity, m^2s^{-1}
θ: thermal resistance, K^{-1}Subscripts
c: copper
i: inlet
o: outlet
w: water